

# Convection in colloidal suspensions with particle-concentration-dependent viscosity

Martin Glässl, Markus Hilt, and Walter Zimmermann<sup>a</sup>

Theoretische Physik I, Universität Bayreuth, 95440 Bayreuth, GERMANY

submitted to European Physical Journal E (received 22 March 2010, received in final form 14 June 2010)

**Abstract.** The onset of thermal convection in a horizontal layer of a colloidal suspension is investigated in terms of a continuum model for binary-fluid mixtures where the viscosity depends on the local concentration of colloidal particles. With an increasing difference between the viscosity at the warmer and the colder boundary the threshold of convection is reduced in the range of positive values of the separation ratio  $\psi$  with the onset of stationary convection as well as in the range of negative values of  $\psi$  with an oscillatory Hopf bifurcation. Additionally the convection rolls are shifted downwards with respect to the center of the horizontal layer for stationary convection ( $\psi > 0$ ) and upwards for the Hopf bifurcation ( $\psi < 0$ ).

**PACS.** 47.20.Bp Buoyancy-driven flows, flow instabilities – 47.57.E- Suspensions, complex fluids – 47.55.P- Buoyancy-driven flows, convection

## 1 Introduction

Rayleigh-Bénard convection [1,2] is a prominent model for many processes in geoscience, atmospheric dynamics, and convection in technical applications [3,4,5]. Moreover it is a classical lab experiment for studying generic phenomena in nonlinear dynamics and pattern formation [5,6]. Typically the Oberbeck-Boussinesq (OB) approximation is used for modeling thermal convection [7,8,9,10]. In this approximation constant material parameters independent of the thermodynamic variables are assumed, except for a temperature-dependent density in front of the gravitational force, which is the essential driving force of convection.

An extension beyond the Boussinesq approximation is accounting for temperature-dependent viscosity which is used, for instance, for modeling various phenomena in the Earth's mantle [11,12,13,14,15,16,17,18,19,20]. A spatially varying viscosity causes additional nonlinear couplings between the temperature and the velocity field and breaks the up-down symmetry of the flow field with respect to the center of the fluid layer. Often this symmetry breaking favors hexagonal patterns near the onset of convection. A linear or sinusoidal temperature dependence of the viscosity causes a reduction of the threshold compared to the case of constant viscosity [11,12,16]. For an exponential temperature dependence of the viscosity one can either have an enhancement or a reduction of the onset of convection, depending on the viscosity contrast, which measures the ratio of the viscosity at the boundaries [15]. Strongly varying material properties in the Earth's mantle

are a major motivation for using a temperature-dependent viscosity in models of thermal convection in single component fluids [18,19,20,21,22]. Materials in the interior of the Earth are however mixtures of several substances. The dependence of the viscosity on the concentration of one component of the mixture and its influence on the onset of convection is one possible effect to be investigated.

An interesting variant of the classical Rayleigh-Bénard system represents thermal convection in binary-fluid mixtures [7]. Here the concentration field of one of the two constituents enters the basic equations as an additional dynamic quantity. Given the possibility of an oscillatory onset of convection, this enriches the bifurcation scenario considerably and accordingly, the system has attracted wide attention by several reasons in the recent decades, including Non-Oberbeck-Boussinesq effects [6,23,24,25,26,27]. In binary-fluid mixtures temperature gradients cause, via the Soret effect, concentration gradients and the concentration field couples via the buoyancy term into the Navier-Stokes equations for the velocity field. In binary-fluid mixtures (*e. g.* alcohol in water) concentration diffusion is roughly a factor of hundred slower than thermal diffusion. For finite amplitudes of the velocity field, this leads to concentration variations in a narrow boundary layer.

In recent experiments Rayleigh-Bénard convection was investigated in colloidal suspensions [28,29,30] with a special focus on Soret driven convection [28,29] and bistable heat transfer, involving new effects like *e. g.* sedimentation [30]. In theoretical studies of convection in colloidal suspensions the model for binary-fluid convection is commonly used considering the colloidal nanoparticles as the second fluid constituent [31]. Since nanoparticles

<sup>a</sup> e-mail: walter.zimmermann@uni-bayreuth.de

are much larger than for instance alcohol molecules in water, their mass diffusion is more than two orders of magnitude smaller. Accordingly the Lewis number of suspensions reaches considerably smaller values, typically in the range of  $10^{-4}$  [32]. The Soret coefficient, representing the strength of the Soret effect, grows linearly with the particle's size [32,33] and can therefore be changed in a wide range by varying mass density and size.

It is well known that the viscosity of a suspension rises with increasing concentration of the solute particles [8, 34, 35]. The concentration of colloidal particles is sensitive to temperature gradients via the Soret effect. Hence variations of the temperature cause spatial variations of the particle concentration. This leads to a spatially varying viscosity which is a function of the local concentration of the colloidal particles. The temperature dependence of the solvent's viscosity is neglected. The goal of this work is the analysis of the onset of convection in a colloidal suspension in terms of a model for binary-fluid mixtures with a special emphasis on the effects of a particle-concentration-dependent viscosity. In Sec. 2 we briefly introduce the underlying equations of motion and the relation between viscosity and particle concentration. The linear stability analysis of the linear heat conducting state and the phase diagrams for the onset of convection are presented in in Sec. 3. Our results are discussed and summarized in Sec. 4.

## 2 Model

Thermal convection in a horizontal layer of colloidal suspensions is described by the common mean field approach for binary-fluid mixtures [7, 24, 25, 26, 27, 36] with one extension: We take into account a linear dependence of the viscosity on the local concentration of colloidal particles.

Assuming that the mass density of the colloidal particles  $\rho_c$  is similar to the mass density of the solvent  $\rho_s$ , *i. e.*

$$\varepsilon = \frac{\rho_c}{\rho_s} \simeq 1, \quad (1)$$

the difference between  $\rho_s$  and the mean density of the suspension  $\rho_0$  is small and therefore sedimentation effects are negligible. In our case a spatially varying mass fraction of the colloidal particles  $N(\mathbf{r}, t)$  causes a spatially varying viscosity similar to Einstein's law [8]:

$$\eta = \eta_0 \left( 1 + \varepsilon \frac{5}{2} (N - N_0) \right). \quad (2)$$

Effects of higher order in  $N(\mathbf{r}, t)$  are neglected [35,37]. Here  $N_0$  represents the mean mass fraction of the colloidal particles and  $\eta_0$  describes the mean viscosity of the suspension.

The common set of basic transport equations for incompressible binary-fluid mixtures, cf. Refs. [7, 24, 25, 26, 27], involves the density of the mixture  $\rho(\mathbf{r}, t)$ , the fluid velocity  $\mathbf{v}(\mathbf{r}, t)$ , the temperature field  $T(\mathbf{r}, t)$ , the mass fraction of the particles  $N(\mathbf{r}, t)$ , and the pressure field  $p(\mathbf{r}, t)$ :

$$\nabla \cdot \mathbf{v} = 0, \quad (3a)$$

$$(\partial_t + \mathbf{v} \cdot \nabla) T = \chi \nabla^2 T, \quad (3b)$$

$$(\partial_t + \mathbf{v} \cdot \nabla) N = D \left[ \nabla^2 N + \frac{k_T}{T_0} \nabla^2 T \right], \quad (3c)$$

$$(\partial_t + \mathbf{v} \cdot \nabla) \mathbf{v} = -\frac{1}{\rho_0} \nabla p + \nabla \cdot (\nu \nabla) \mathbf{v} + \frac{\rho}{\rho_0} \mathbf{g}. \quad (3d)$$

Eq. (3a) describes the incompressibility of the fluid.  $\chi$  in the heat equation (3b) denotes the thermal diffusivity of the mixture and  $D$  in the diffusion equation (3c) the diffusion constant. Due to the size of the colloidal particles  $D$  takes much smaller values than in molecular fluid mixtures. The dimensionless thermal-diffusion ratio  $k_T$  representing the cross coupling between the temperature gradient and the particle flux is related to the Soret coefficient  $S_T$  via  $k_T = N(1 - N)TS_T$  and can be either positive or negative. In the following  $k_T \simeq N_0(1 - N_0)T_0S_T$  is regarded as constant. In our model the kinematic viscosity  $\nu = \eta/\rho_0$  in the Navier-Stokes-equations (3d) is a function of space, as introduced by Eq. (2). The gravity field  $\mathbf{g} = -g\mathbf{e}_z$  is chosen parallel to the z-direction.

For the local density  $\rho$  of the suspension we use a linearized equation of state [7, 10],

$$\rho = \rho_0 [1 - \alpha(T - T_0) + \beta(N - N_0)], \quad (4)$$

with the thermal expansion coefficient  $\alpha = -(1/\rho_0)\partial\rho/\partial T$  and  $\beta = (1/\rho_0)\partial\rho/\partial N$  reflecting the density contrast between the solvent and the suspended particles. According to the Boussinesq approximation this dependency of the density is taken into account only within the buoyancy term. The sign of  $\beta$  indicates whether the colloidal particles have a higher or a lower mass density than the solvent. Here we assume  $\beta > 0$ , corresponding to  $\varepsilon > 1$ .

*Boundary conditions.* The fluid layer is confined between two impermeable and parallel plates at a distance  $d$ , and extends infinitely in the  $(x, y)$ -plane. The lower plate ( $z = -d/2$ ) is kept at a higher temperature  $T_0 + \delta T/2$ , the upper plate ( $z = +d/2$ ) at a lower temperature  $T_0 - \delta T/2$ .

Considering realistic no-slip boundary conditions for the flow field the boundary conditions at  $z = \pm d/2$  are:

$$0 = v_x = v_y = v_z = \partial_z v_z, \quad (5a)$$

$$0 = \partial_z N + \frac{k_T}{T_0} \partial_z T, \quad (5b)$$

$$T = T_0 \mp \frac{\delta T}{2}. \quad (5c)$$

For geophysical applications free-slip boundary conditions

$$0 = \partial_z v_x = \partial_z v_y = v_z = \partial_z^2 v_z, \quad (6)$$

for the flow field are often considered to be more realistic [21]. In the case of constant viscosity and free-slip boundary conditions an analytical determination of the onset of convection is possible [25]. This advantage is lost when introducing a concentration dependent viscosity and one has to rely on numerical methods.

*Basic state.* In the absence of convection ( $\mathbf{v} = 0$ ) the time-independent heat-conducting state is described by:

$$T_{cond} = T_0 - \delta T \frac{z}{d}, \quad (7a)$$

$$N_{cond} = N_0 - \delta N \frac{z}{d} \quad \text{with} \quad \delta N = -\frac{k_T}{T_0} \delta T. \quad (7b)$$

For further analysis it is convenient to separate the basic heat-conducting state in Eq. (7) from convective contributions of the temperature and concentration fields as follows:  $T(\mathbf{r}, t) = T_{cond}(z) + T_1(\mathbf{r}, t)$  and  $N(\mathbf{r}, t) = N_{cond}(z) + N_1(\mathbf{r}, t)$ .

Since we have rotational symmetry in the fluid layer we can restrict our further analysis concerning the onset of convection to two spatial dimensions, namely to the  $(x, z)$ -plane. With this simplification the fluid velocity can be expressed by a *stream function*  $\Phi(x, z, t)$ :

$$\tilde{v}_z = \partial_x \Phi, \quad \tilde{v}_x = -\partial_z \Phi. \quad (8)$$

Subsequently all lengths are scaled by the distance  $d$  and time by the vertical thermal diffusion time  $d^2/\chi$ . Scaling the temperature field  $T$  by  $(\chi\nu_0)/(\alpha g d^3)$ , the concentration field  $N$  by  $-(k_T \chi \nu_0)/(T_0 \alpha g d^3)$  and the stream function  $\Phi$  by  $\chi d$  we are left with *five dimensionless parameters*: The *Rayleigh number*  $R$ , the *Prandtl number*  $P$ , the *Lewis number*  $L$ , and the *separation ratio*  $\psi$ ,

$$P = \frac{\nu_0}{\chi}, \quad L = \frac{D}{\chi}, \quad R = \frac{\alpha g d^3}{\chi \nu_0} \delta T, \quad \psi = \frac{\beta k_T}{\alpha T_0}, \quad (9)$$

are well known from molecular binary-fluid mixtures [26, 27]. The fifth dimensionless quantity

$$Q = \varepsilon \frac{5}{2} \frac{\nu_0 \chi}{g \beta d^3} \quad (10)$$

is introduced to characterize the spatially varying contribution to the viscosity of the suspension. For small particles in water a reasonable value is  $Q \simeq 0.01$  and for glycerin  $Q \simeq 10$ . A further illustration of its physical meaning is obtained by considering the viscosity contrast  $\tilde{\eta} = \eta(z = +\frac{1}{2})/\eta(z = -\frac{1}{2})$  between the concentration-dependent viscosity at the upper and the lower boundary,

$$\tilde{\eta} = \frac{1 + \frac{5\varepsilon}{4T_0} k_T \delta T}{1 - \frac{5\varepsilon}{4T_0} k_T \delta T} = \frac{1 + \frac{1}{2} R \psi Q}{1 - \frac{1}{2} R \psi Q}, \quad (11)$$

which is essentially a function of the product of the three dimensionless control parameters:  $R \psi Q$ . In the following we will discuss our results essentially in dependence of  $\psi$  and  $Q$  whereas  $P$  and  $L$  are regarded as constants.

For further analysis we introduce a rescaled temperature deviation  $\theta = (R/\delta T)T_1$  and a rescaled concentration deviation  $\tilde{N}_1 = -(T_0 R/k_T \delta T)N_1$  in terms of these dimensionless quantities. In addition it is advantageous to introduce the combined function  $\tilde{c} = \tilde{N}_1 - \theta$  instead of  $\tilde{N}_1$ .

Suppressing for reasons of simplicity all the tildes we obtain:

$$(\partial_t - \Delta)\theta - R\partial_x \Phi = (\partial_z \Phi \partial_x - \partial_x \Phi \partial_z)\theta, \quad (12a)$$

$$(\partial_t - L\Delta)c + \Delta\theta = (\partial_z \Phi \partial_x - \partial_x \Phi \partial_z)c, \quad (12b)$$

$$\begin{aligned} (\partial_t - P\Delta)\Delta\Phi - P\psi\partial_x c - P(1+\psi)\partial_x \theta \\ - \psi PQR[z\Delta + 2\partial_z] \Delta\Phi = (\partial_z \Phi \partial_x - \partial_x \Phi \partial_z)\Delta\Phi \\ - \psi PQ [\partial_x^2(c + \theta)\partial_x^2\Phi + 2\partial_x \partial_z(c + \theta)\partial_x \partial_z \Phi \\ + \partial_z^2(c + \theta)\partial_z^2\Phi]. \end{aligned} \quad (12c)$$

No-slip, impermeable boundary conditions for the fields  $\theta$ ,  $c$ , and  $\Phi$  demand

$$\theta = \partial_z c = \Phi = \partial_z \Phi = 0 \quad \text{at } z = \pm \frac{1}{2}. \quad (13)$$

while free-slip, permeable boundary conditions [25, 36, 38]

$$\theta = c = \Phi = \partial_z^2 \Phi = 0 \quad \text{at } z = \pm \frac{1}{2}. \quad (14)$$

All results presented in this work base upon calculations with no-slip, impermeable boundary conditions. However, free-slip permeable boundary conditions lead to qualitatively comparable behavior.

### 3 Linear stability of the heat conducting state and the onset of convection.

The critical values of the control parameters at the onset of convection are determined by investigating the growth dynamics of small perturbations  $\theta(x, z, t)$ ,  $c(x, z, t)$ , and  $\phi(x, z, t)$  with respect to the heat conducting state given by Eqs. (7). The dynamics of such small perturbations is governed by the linear parts of the coupled nonlinear equations (12). They are solved by the following exponential ansatz with respect to time  $t$  and the horizontal  $x$ -direction:

$$\begin{pmatrix} \theta(x, z, t) \\ c(x, z, t) \\ \phi(x, z, t) \end{pmatrix} = \mathbf{u}_0(z) e^{iqx} e^{\sigma t}, \quad (15)$$

$$\text{with} \quad \mathbf{u}_0(z) = \begin{pmatrix} \bar{\theta}(z) \\ \bar{c}(z) \\ \bar{\phi}(z)/(iq) \end{pmatrix}. \quad (16)$$

With this ansatz and the eigenvalue  $\sigma$  the linear parts of Eqs. (12) are transformed into a boundary eigenvalue-problem with respect to  $z$ . The remaining linear ordinary differential equations (ODEs) are solved in this work by two different methods.

The first one is a standard *shooting method* as described in detail for binary-fluid convection in Ref. [27]: The resulting coupled ODEs for  $\mathbf{u}_0(z)$  are integrated by a standard solver for ODEs. For every set of initial conditions a boundary determinant  $f(\sigma, R, q, Q, P, L, \psi)$  is calculated. During an iteration procedure  $R$  or  $\sigma$  are varied

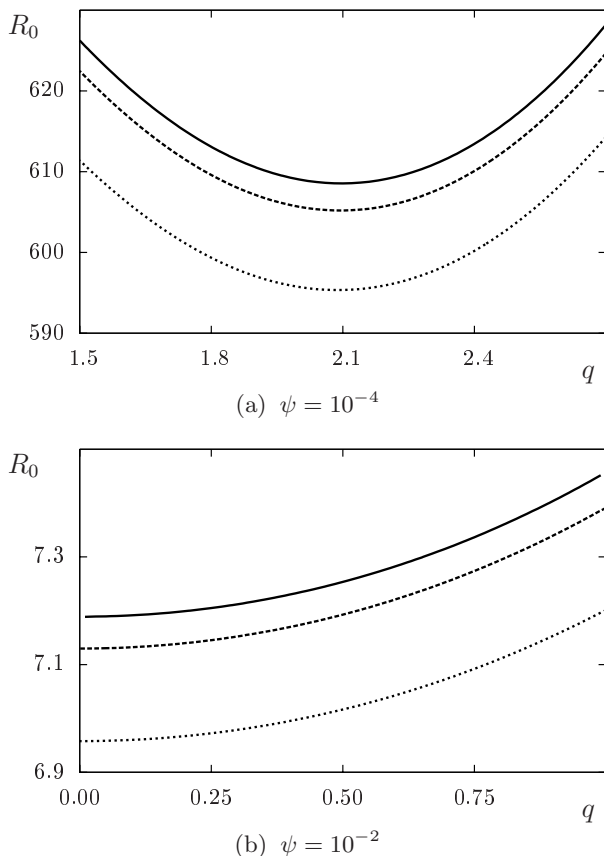


**Fig. 1.** Neutral curves  $R_0(q)$  obtained according to Eq. (17) are shown for different values of the viscosity parameter,  $Q = 0$  (solid line),  $Q = 5$  (dashed line) and  $Q = 10$  (dotted line). In part a) for the positive separation ratio  $\psi = 10^{-4}$  and in b) for  $\psi = 10^{-2}$ .

such that  $f$  vanishes. This yields  $\sigma$  and  $R$  as a function of the remaining parameters.

The second possibility is the so-called *Galerkin method* where the components of  $\mathbf{u}_0(z)$  are expanded with respect to a suitable chosen set of functions which fulfill the boundary conditions, either Eq. (13) or Eq. (14) - see, *e. g.*, Ref. [39, 40, 41]. Here the linear ODEs are transformed into a generalized algebraic eigenvalue problem which can be solved numerically.

At the onset of convection small perturbations  $\theta$ ,  $c$ , and  $\phi$  with respect to the linear ground state neither grow nor decay, i. e. we are interested in the neutral stability condition for the fastest growing mode (eigenvalue  $\sigma$  with the largest real part),

$$\text{Re}(\sigma) = 0 \quad \text{with} \quad \sigma = \sigma(R, q, Q, P, L, \psi), \quad (17)$$

for the determination of the threshold. Depending on parameters the system may show a stationary bifurcation with a vanishing imaginary part of the eigenvalue,  $\text{Im}(\sigma) = \omega = 0$ , or a Hopf bifurcation with a finite Hopf frequency  $\text{Im}(\sigma) = \pm\omega \neq 0$ .

For a given set of material parameters the neutral stability condition (17) provides the Rayleigh number  $R_0(q)$

as a function of  $q$ , the so-called *neutral curve*

$$R_0(q) = R_0(q, Q, P, L, \psi). \quad (18)$$

Similarly we obtain from Eq. (17)  $\omega_0 = \omega_0(q, Q, P, L, \psi)$  in the case of a Hopf bifurcation.

In this work we choose a Prandtl number of  $P = 10$ . Since the mass diffusion of the colloidal particles is much lower than the thermal diffusion, a Lewis number of  $L = 10^{-4}$  is a reasonable assumption. For small particles in water  $Q \simeq 0.01$  and in Glycerin  $Q \simeq 10$  are appropriate values. As the main changes for finite values of  $Q$  occur if  $\psi$  is comparable to  $L$  we concentrate on rather small values of  $\psi$ .

Neutral curves for the present system are given in Fig. 1 for two different positive values of the separation ratio  $\psi$ , namely for  $\psi = 10^{-4}$  and  $\psi = 10^{-2}$ , and for three different values of the viscosity parameter  $Q = 0, 5, 10$ . The onset of convection is given by the minimum of the neutral curves  $R_c = R_0(q_c) = \min R_0(q)$  which can be compared with its corresponding value in the case of a simple Newtonian fluid,  $R_c^{NF} \simeq 1708$ , and molecular binary mixtures [27].

The reduction of the threshold in the range of  $\psi > 0$  is well known from molecular binary fluids [25, 27] and the reason is as follows. Due to thermal expansion a fluid layer heated from below becomes lighter at the lower boundary and there is a temperature induced density gradient. According to a positive Soret effect ( $\psi > 0$ ) the colloidal particles tend to move to the upper plate which is colder. As the colloids are heavier than the molecules of the solvent the Soret induced concentration gradient amplifies the temperature induced density gradient. Hence the fluid layer becomes unstable already at temperature differences much lower than for the onset of convection in a simple fluid.

For positive values of  $\psi$ , shown in Fig. 1, the bifurcation from the heat conducting state is stationary. While the minimum of the neutral curve is located at a finite wavenumber  $q_c > 0$  for values of  $\psi$  that are small compared to  $L$  (cf. Fig. 1(a)), the critical wavenumber moves to  $q_c = 0$  for larger values of  $\psi$  (cf. Fig. 1(b)). Finite values of  $Q$  lead to a lowering of the neutral curves whereby the critical wavenumber is nearly unaffected. The differences between the critical wavenumbers  $q_c$  at the minimum of the neutral curves in Fig. 1(a) is less than 0.1%.

Fig. 2 shows the threshold reduction as a function of  $Q$  for three different positive values of  $\psi$ . Here we plot the critical Rayleigh number  $R_c(Q)$  normalized by the critical Rayleigh number  $R_c(Q = 0)$  which we call the relative critical Rayleigh number

$$R_{c,rel}(Q) = \frac{R_c(Q)}{R_c(Q = 0)}. \quad (19)$$

The reduction of  $R_{c,rel}(Q)$  as a function of  $Q$  shows a parabola-like behavior as shown in Fig. 2, which is accompanied by a tiny variation of the critical wavenumber  $q_c$  along each curve.

For finite values of  $\psi$  the ground state displays a viscosity contrast  $\tilde{\eta} \neq 0$  as described by Eq. (11). Fig. 3 shows



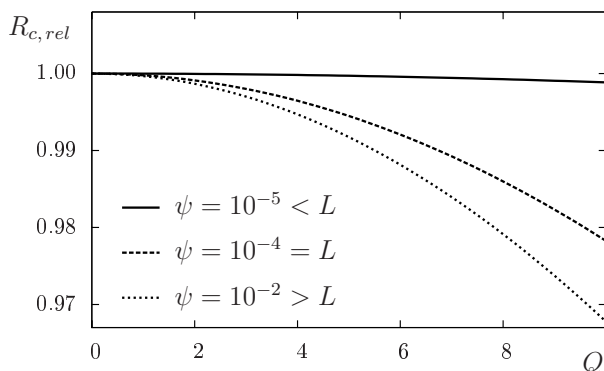


**Fig. 2.** The relative critical Rayleigh number  $R_{c,rel} = R_c(Q)/R_c(Q=0)$  is shown as a function of  $Q$  for three different values of the separation ratio  $\psi$ : For  $\psi = 10^{-5} < L$  (solid) one has  $q_c = 2.97$ , for  $\psi = 10^{-4} = L$  (dashed)  $q_c = 2.10$  and for  $\psi = 10^{-2} > L$  (dotted)  $q_c = 0.00$ .

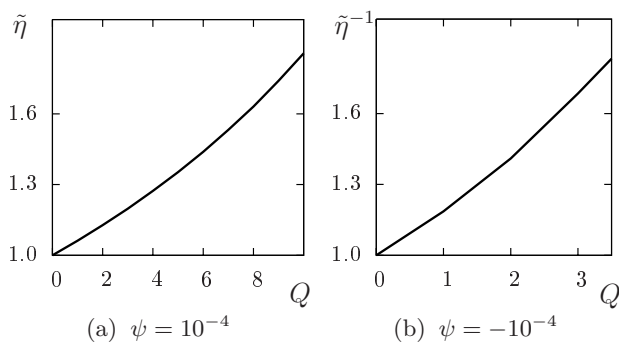


**Fig. 3.** In part (a) the viscosity contrast  $\tilde{\eta}$ , given by Eq. (11), is plotted for  $\psi = 10^{-4}$  and in part b) the inverse expression  $\tilde{\eta}^{-1}$  is plotted for  $\psi = -10^{-4}$ . In both cases the Rayleigh number  $R$  entering Eq. (11) was taken at the respective onset of convection.

$\tilde{\eta}(Q)$  as a function of  $Q$  for two different values of  $\psi$  at the onset of convection  $R = R_c$ . The  $Q$ -range in Fig. 3 was limited to the range  $|RQ\psi| \leq 1/4$  where  $k_T = \text{const.}$  is a reasonable assumption.

Another interesting question is how the threshold reduction behaves as function of the viscosity contrast  $\tilde{\eta}$ . Within our model the viscosity depends linearly on the concentration, according to Eq. (2). Since the concentration, via Eq. (7b), is a linear function of the temperature, the viscosity is effectively a linear function of the temperature too. For a given viscosity contrast the threshold reduction of stationary convection ( $\psi > 0$ ) is similar to that in a previous study of a single component fluid with a direct linear temperature dependence of the viscosity [16]. However, there are important differences between this single component study and the present model: Here the viscosity contrast is caused by a well known physical mechanism, the Soret effect. The viscosity contrast is accompanied by heterogeneous distributions of the colloidal particles, which can be of relevance in the context of related convection phenomena in geoscience. For a single component fluid in Ref. [16] one has only a stationary onset of convection. In contrast the concentration field for the colloidal particles represents an additional degree of

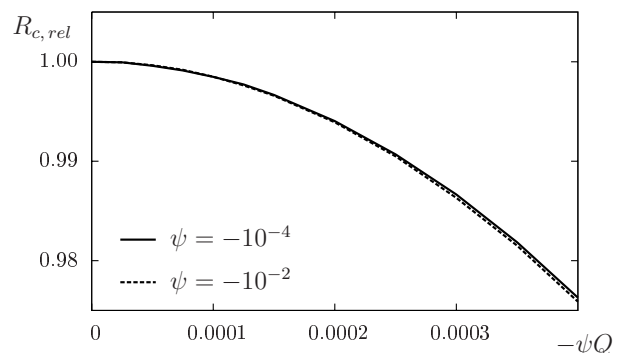


**Fig. 4.** The relative critical Rayleigh number  $R_{c,rel} = R_c(Q)/R_c(Q=0)$  is shown as function of the product  $-\psi Q$  for two different values of the separation ratio  $\psi$ : For  $\psi = -10^{-4}$  (solid) and for  $\psi = -10^{-2}$  (dashed). The critical wavenumber along both curves takes the value  $q_c \simeq 3.116$ .

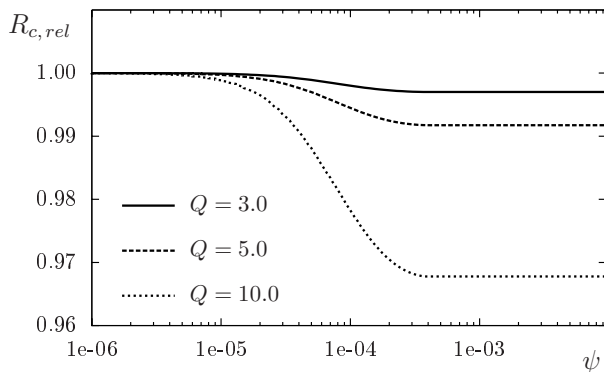
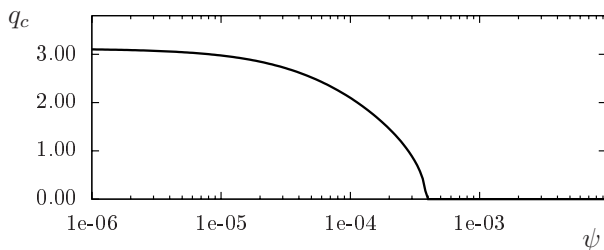
freedom which, in the range of  $\psi < 0$ , similar as in molecular binary-fluid mixtures [25,27], leads to an oscillatory onset of convection via a Hopf bifurcation.

Therefore arises a further interesting question: How does a finite viscosity contrast affect an oscillatory bifurcation? We find in the range of  $\psi < 0$ , as in the range of  $\psi > 0$ , a lowering of the neutral curve with increasing values of  $Q$ . The critical wavenumber  $q_c$ , as well as the Hopf frequency  $\omega_c$ , show only small and negligible changes when varying  $Q$ . The  $Q$  dependence of the relative critical Rayleigh number  $R_{c,rel}(Q)$  is slightly different from its behavior in the positive range of  $\psi$ . For  $\psi > 0$  the critical Rayleigh number  $R_c(\psi)$  decays strongly as a function of  $\psi$ , whereas the threshold increases only moderately for decreasing  $\psi$  in the range  $\psi < 0$  [25,27]. Therefore, the viscosity contrast at threshold given by Eq. (11) is for  $\psi < 0$  essentially a function of the product  $\psi Q$ .

The relative threshold  $R_{c,rel}(Q\psi)$  is shown in Fig. 4 as a function of the product  $-Q\psi$  for two different values of  $\psi < 0$ . The two curves are nearly identical as expected. Therefore, the changes of the threshold of the oscillatory convection are again essentially determined by the viscosity contrast  $\tilde{\eta}$  given by Eq. (11) in the restricted range  $|R\psi Q| \leq 1/4$ .

Another view on the parameter dependence of the threshold is given in Fig. 5, where the relative critical Rayleigh number  $R_{c,rel}(\psi)$  is shown as a function of the separation ratio  $\psi$  for three different values of the viscosity parameter  $Q = 3.0, 5.0, \text{ and } 10.0$ . In the limit of a vanishing separation ratio  $\psi$  the particle concentration and therefore the viscosity contrast  $\tilde{\eta}$  does not change by varying  $Q$ , so we have  $R_{c,rel} \simeq 1$ . For increasing values of  $\psi$  the threshold drops down and finally reaches a constant value, depending on  $Q$ . The strongest decay can be observed in the region  $\psi \simeq L$  accompanied by the critical wavenumber  $q_c$  going down.  $q_c$  finally vanishes at nearly the same value of  $\psi \simeq 4 \times 10^{-4}$  independently of  $Q$  as shown by Fig. 5b).

For  $\psi > 0$  an increasing viscosity contrast leads to a decrease of the velocity field at the upper boundary as the fluid motion tends to concentrate in the region of lower viscosity at the lower boundary. Therefore the center of

(a)  $R_{c,rel}(\psi, Q)$ (b)  $q_c(\psi)$ 

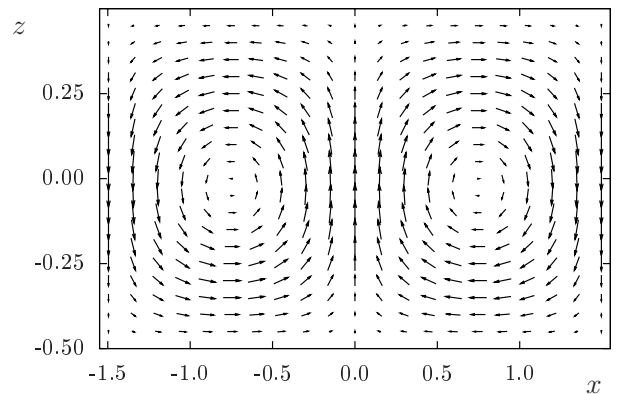
**Fig. 5.** Part a) shows the relative critical Rayleigh number  $R_{c,rel}(\psi, Q) = R_c(\psi, Q)/R_c(\psi, Q = 0)$  as a function of the separation ratio  $\psi$  for three different values of  $Q$ :  $Q = 3.0$  (solid),  $Q = 5.0$  (dashed), and  $Q = 10.0$  (dotted). Part b) shows the corresponding critical wavenumber  $q_c(\psi)$ .

the convection rolls at  $z_0$  is slightly shifted below the center of the convection cell at  $z = 0$  as shown in Fig. 6a) for  $\psi = 10^{-4}$ . This shift  $z_0$  is more clearly indicated in Fig. 6b), which shows the horizontal component of the convection velocity,  $v_x(z)$ , as function of  $z$ . The shift  $z_0$  to negative values increases with increasing values of  $Q$  as shown in Fig. 6c). This behavior is common for all positive values of  $\psi$  with a finite value of the critical wavenumber  $q_c$ . For  $\psi < 0$ , in the range of an oscillatory Hopf bifurcation, the viscosity is higher at the lower boundary and therefore the magnitude of the velocity is reduced near the lower plate. Accordingly, the center of the convection rolls,  $z_0$ , is elevated with increasing values of  $\psi Q$  to  $z_0 > 0$ . Our analysis shows that the shift  $|z_0|$  depends essentially on the viscosity contrast  $\tilde{\eta}$ .

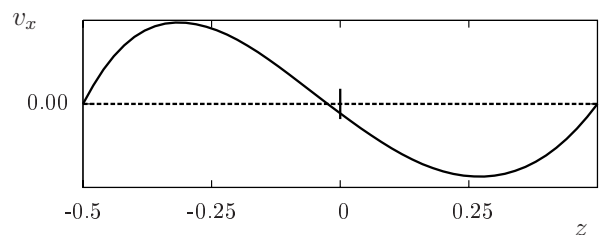
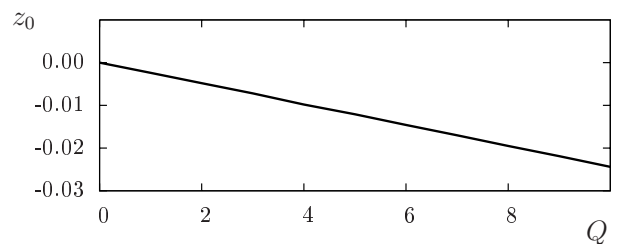
Assuming free-slip boundary conditions (14) instead of no-slip boundary conditions (13), we obtain very similar results. For finite values of  $Q$  the threshold is reduced compared to its value at  $Q = 0$  and the center of the rolls is shifted to the region of lower viscosity.

## 4 Conclusions

The onset of thermal convection in a colloidal suspension was investigated in terms of a generalized continuum model for binary-fluid mixtures going beyond the common Boussinesq-approximation by taking into account a linear



(a) velocity field

(b)  $v_x(z)$ (c)  $z_0$  at  $v_x(z_0) = 0$ 

**Fig. 6.** The flow velocity field at the onset of stationary convection is shown in part a) for the parameters  $\psi = 10^{-4}$  and  $Q = 10$ . Part b) depicts the variation of the velocity component  $v_x(z)$  for the same parameters as a function of the vertical coordinate  $z$  and part c) shows the shift of the position  $z_0$  where the horizontal velocity vanishes, *i. e.*  $v_x(z_0) = 0$ , as a function of  $Q$ .

dependency of the viscosity on the local concentration of the colloidal particles.

Spatial changes of the concentration of colloidal particles in the convection cell are induced by temperature variations via the Soret effect similar to that in molecular binary-fluid mixtures. The influence of the particle concentration on the viscosity is described by a dimensionless viscosity parameter  $Q$ , introduced in this work. For finite values of  $Q$  the threshold is reduced compared to the limit  $Q = 0$ , for both the stationary bifurcation for  $\psi > 0$  and the oscillatory Hopf bifurcation for  $\psi < 0$ . This reduction depends essentially on the induced viscosity contrast  $\tilde{\eta}$  at the chosen values of  $Q$  and  $\psi$ . We would like to emphasize that  $|R\psi Q|$  may not be too large so that the linear approximation of the concentration variation in Eq. (7b) remains a reasonable assumption.

For both bifurcations the center of the convection rolls is shifted slightly away from the center of the convection cell: For  $\psi > 0$  the convection rolls are shifted below and for  $\psi < 0$  beyond the center of the cell, as the fluid motion always tends to concentrate in the region of lower viscosity. At the onset of convection the changes of the critical wavenumber of the convection rolls as a function of the dimensionless parameter  $Q$  are rather small.

In a previous study on convection for a single component fluid in Ref. [16] a linear dependence of the viscosity on the temperature was assumed and its influence on the onset of stationary convection was investigated. Assuming the same viscosity contrast a similar relative reduction in the threshold is obtained as in our model. However, our model does not only describe a spatial variation of the material parameters. It describes also a mechanism leading, via a heterogeneous concentration distribution, to a spatial dependence of the viscosity. This interrelation between concentration and viscosity variations may be of relevance to related phenomena in geophysical contexts. Additionally, the further degree of freedom in our model, introduced by the concentration dynamics, provides a richer bifurcation scenario and we can investigate the effects of a spatially varying viscosity on a stationary as well as on a Hopf bifurcation.

In this work the viscosity  $\hat{\eta}_0$  of the solvent of the colloidal particles was assumed to be constant. A natural extension of the present model would be to take also into account the effects of a temperature-dependent viscosity of the carrier fluid. In the range of larger values of  $\psi > 0$  with small temperature differences at the threshold, this effect may be small. However, in the range of small and negative values of  $\psi$  this effect may play a role and one may then have a spatially varying mobility of the colloidal particles corresponding to a temperature and spatially dependent Lewis number. A temperature dependent Lewis number is also expected for thermosensitive microgel suspensions [42,43] in which core-shell colloids change their size as a function of the temperature and their mobility as well as the viscosity of the suspension. This combined effect on the viscosity as well as the effects of nonlinear variations of the particle concentration will be discussed elsewhere.

The vertical viscosity variation, caused by a temperature gradient and leading to spatially dependent viscosity, breaks the up-down symmetry in the convection cell. Therefore the interesting question arises: In which parameter range are hexagonal patterns favored for this binary-fluid model in the weakly nonlinear regime?

Stimulating discussions with F. H. Busse, M. Evonuk, G. Freund, W. Köhler, W. Pesch, I. Rehberg, and W. Schöpf are appreciated. This work has been supported by the German science foundation through the research unit FOR 608.

## References

1. H. Bénard, Gén. Sci. Pures Appl. **11**, 1261 and 1309 (1900).
2. L. Rayleigh, Phil. Mag. **32**, 529 (1916).
3. W. R. Cotton, G. Bryan, and S. V. den Heever, *Storm and Cloud Dynamics* (Academic Press, New York, 2010).
4. R. A. Houze, *Cloud Dynamics* (Academic Press, New York, 1994).
5. E. Bodenschatz, W. Pesch, and G. Ahlers, Annu. Rev. Fluid Mech. **32**, 709 (2000).
6. M. C. Cross and P. C. Hohenberg, Rev. Mod. Phys. **65**, 851 (1993).
7. J. K. Platten and L. C. Legros, *Convection in Liquids* (Springer, Berlin, 1984).
8. L. D. Landau and E. M. Lifschitz, *Course in Theoretical Physics: Fluid Dynamics* (Butterworth, Boston, 1987).
9. F. H. Busse, in *Mantle Convection: Plate Tectonics and Global Dynamics*, edited by W. R. Peltier (Gordon and Breach, Montreux, 1989), pp. 23–95.
10. G. Z. Gershuni and E. M. Zhukhovitskii, *Convective Stability of Incompressible Fluids* (Keter, Jerusalem, 1976).
11. E. Palm, J. Fluid Mech. **8**, 183 (1960).
12. O. Jensen, Acta Polytech. Scand. **24**, 1 (1963).
13. K. E. Torrance and D. L. Turcotte, J. Fluid Mech. **47**, 451 (1970).
14. J. R. Booker, J. Fluid Mech. **76**, 741 (1976).
15. K. C. Stengel, D. S. Oliver, and J. R. Booker, J. Fluid Mech. **120**, 411 (1982).
16. F. H. Busse and H. Frick, J. Fluid Mech. **150**, 451 (1985).
17. D. B. White, J. Fluid Mech. **191**, 247 (1988).
18. U. R. Christensen and H. Harder, Geophys. J. Int. **104**, 213 (1991).
19. S. Balachandar, D. A. Yuen, D. M. Reuteler, and G. S. Lauer, Science **267**, 1150 (1995).
20. P. Tackley, J. Geophys. Res. **101**, 3311 (1996).
21. M. Ogawa, G. Schubert, and A. Zebib, J. Fluid Mech. **233**, 299 (1991).
22. M. Ogawa, Fluid Dyn. Res. **40**, 379 (2008).
23. S. J. Linz and M. Lücke, Phys. Rev. A **36**, 3505 (1987).
24. M. Lücke *et al.*, in *Evolution of Spontaneous Structures in Dissipative Continuous Systems*, edited by F. H. Busse and S. C. Müller (Springer, Berlin, 1998).
25. H. R. Brand, P. C. Hohenberg, and V. Steinberg, Phys. Rev. A **30**, 2548 (1984).
26. M. C. Cross and K. Kim, Phys. Rev. A **38**, 529 (1988).
27. W. Schöpf and W. Zimmermann, Phys. Rev. E **47**, 1739 (1993).
28. R. Cerbino, A. Vailati, and M. Giglio, Phys. Rev. E **66**, 055301 (2002).
29. R. Cerbino, S. Mazzoni, A. Vailati, and M. Giglio, Phys. Rev. Lett. **94**, 064501 (2005).
30. G. Donzelli, R. Cerbino, and A. Vailati, Phys. Rev. Lett. **102**, 104503 (2009).
31. B. Huke, H. Pleiner, and M. Lücke, Phys. Rev. E **75**, 036203 (2007).
32. R. Piazza and A. Parola, J. Phys. Condens. Matter **20**, 153102 (2008).
33. S. Duhr and D. Braun, Phys. Rev. Lett. **96**, 168301 (2006).
34. A. Einstein, Ann. d. Physik **19**, 289 (1906).
35. R. G. Larson, *The Structure and Rheology of Complex Fluids* (Oxford Press, Oxford, 1999).
36. D. Guthkowitz-Krusin, M. A. Collins, and J. Ross, Phys. Fluids **22**, 1443; **22** 1451 (1979).
37. G. K. Batchelor and J. T. Green, J. Fluid Mech. **56**, 401 (1972).

38. W. Hort, S. J. Linz, M. Lücke, *Phys. Rev. A* **45**, 3737 (1992).
39. W. Pesch, *Chaos* **6**, 348 (1996).
40. R. M. Clever and F. H. Busse, *J. Fluid Mech.* **65**, 625 (1974).
41. C. Canuto, M. Y. Houssanini, A. Quarteroni, and T. A. Zang, *Springer Series in Computational Physics* (Springer-Verlag, Berlin 1987).
42. M. Ballauff and Y. Lu, *Polymer* **48**, 1815 (2007).
43. F. Winkel, S. Messlinger, W. Schöpf, I. Rehberg, M. Siebenbürger, and M. Ballauf, *New J. Phys.* **12**, 053003 (2010).